PROCEEDINGS OF SCIENCE

Deeply Virtual Compton Scattering at 11GeV in Jefferson Lab Hall A

Frédéric Georges[*†]
Institut de Physique Nucléaire d'Orsay
E-mail: georges@ipno.in2p3.fr

Introduced in the mid 90's, Generalized Parton Distributions (GPDs) are now a key element in the study of the nucleon internal structure. Indeed, GPDs encapsulate both spatial and momentum distributions of partons inside a nucleon. Through the Ji sum rule, they also allow to derive the total orbital angular momentum of quarks, which is a crucial point to unravel the nucleon spin structure.
GPDs are experimentally accessible through Deeply Virtual Compton Scattering (DVCS) and its interference with the Bethe-Heitler process at high momentum transfer Q^2. A worldwide experimental program was started in the early 2000's to extract these GPDs. The subject of this document, a DVCS $ep \to e'p'\gamma$ experiment performed at Jefferson Laboratory, Hall A (Virginia, USA) between 2014 and 2016, is encompassed in this program.
The aim of this experiment is to extract with high precision the DVCS helicity-dependent cross sections as a function of the momentum transfer Q^2, for fixed values of the Bjorken variable x_{Bj}, on a proton target. The recent upgrade of the accelerator facility to 12 GeV allows to cover a larger Q^2 lever arm than for previous measurements and probe yet unexplored kinematic regions, while the polarized electron beam will allow the separation of the contributions from the real and imaginary parts of the DVCS amplitude to the total cross section.
This document will give an overview of the ongoing data analysis for this experiment, followed by the presentation of the obtained preliminary results.

23rd International Spin Physics Symposium - SPIN2018 -
10-14 September, 2018
Ferrara, Italy

[*]Speaker.
[†]For the Jefferson Lab Hall A collaboration

PoS(SPIN2018)072

1. Accessing Generalized Partons Distributions through DVCS

A large number of experiments have already been made in order to study the internal structure of the proton. Elastic scattering $ep \to e'p'$ gives access to elastic form factors, which provide information about the spatial distribution of partons inside of the proton. Deep Inelastic Scattering (DIS) $ep \to e'X$ gives access to partons distribution functions, which yield information about the momentum distribution of partons inside of the proton. However, such measurements cannot provide information about the correlations between spatial and momentum distributions of partons, and as such, our understanding of the proton internal structure remains incomplete.

In the early 2000's, the Deeply Virtual Compton Scattering (DVCS) $ep \to e'p'\gamma$ process started to gather a lot of interest, as it is the cleanest channel to extract Generalized Partons Distributions (GPDs). Introduced in the mid 90's, GPDs provide essential information for the study of the proton internal structure since they give access to the correlations between spatial and momentum distributions of partons, as well as the total orbital angular momentum of quarks through the Ji sum rule [1, 2, 3].

In the Bjorken limit (Eq. (1.1)), the DVCS process can be simplified to the 'Handbag diagram' (see Fig. 1), where an electron is scattering off a single quark of the proton through the exchange of a virtual photon, and after the interaction, the struck quark emits a real photon. This diagram can be factorized into two parts [4, 5]: a hard part which can be computed with perturbative QCD, and a soft part which is parametrized by four quark GPDs $H_q(x,\xi,t)$, $E_q(x,\xi,t)$, $\widetilde{H}_q(x,\xi,t)$, and $\widetilde{E}_q(x,\xi,t)$ (see Fig. 1, left). The measurement of the DVCS cross section allows one to extract information about the GPDs.

$$Q^2 = -q^2 \to \infty \quad ; \quad \nu \to \infty \quad ; \quad x_{Bj} = \frac{Q^2}{2M\nu} \quad fixed. \tag{1.1}$$

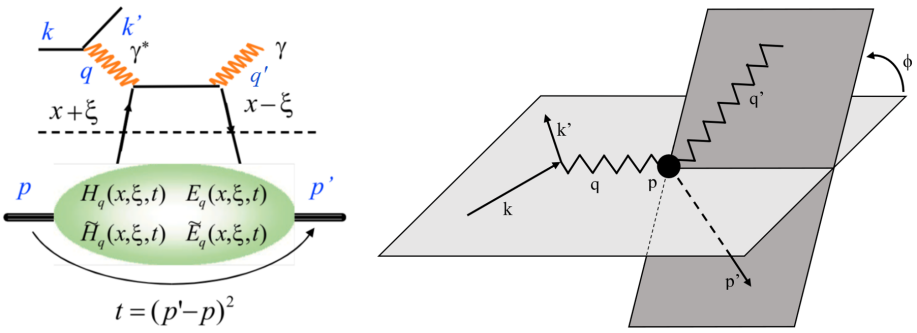

Figure 1: Left: Handbag diagram of the DVCS process. k and k' are the electron four-vectors, p and p' are the proton four-vectors, and q is the virtual photon four-vector. ν is the difference of energy of the electron before and after the interaction. t is the momentum transfer to the proton. $x+\xi$ and $x-\xi$ are the fractions of the proton longitudinal momentum carried by the struck quark before and after the interaction, respectively. Right: Three dimensional representation of the DVCS process. The azimuthal angle ϕ is defined in the Trento convention [6].

Unfortunately, the variable x is not experimentally accessible. In the DVCS amplitude, the GPDs are either integrated over x, or evaluated at $x = \pm\xi$. As a consequence, when studying

GPDs, it is usual to first extract Compton Form Factors (CFFs), which are complex quantities of the form:

$$\mathscr{R}e\mathscr{H}_q(\xi,t) = \mathscr{P}\int_0^1 [H_q(x,\xi,t) - H_q(-x,\xi,t)]\,(\frac{1}{x-\xi}+\frac{1}{x+\xi})dx, \tag{1.2}$$

$$\mathscr{I}m\mathscr{H}_q(\xi,t) = -\pi\,(H_q(\xi,\xi,t) - H_q(-\xi,\xi,t))\,, \tag{1.3}$$

where $\mathscr{P}$ is the principal value integral.

The limit $Q^2 \to \infty$ is required to ensure the interaction of the electron with a single parton of the proton. As this limit cannot be met in practice, corrections for interactions with additional partons might be required. The twist allows to characterize these additional interactions: the leading twist of DVCS (see Fig. 1, left) is equal to 2, and higher twist corrections are suppressed by increasing powers of $\frac{1}{Q}$ with respect to the leading twist.

Experimentally, it is not possible to distinguish DVCS from the Bethe-Heitler process since they have the same initial and final state, although in the Bethe-Heitler case the real photon is emitted by the electron instead of a quark. As a consequence, the cross section measured experimentally is the sum of a DVCS term, a Bether-Heitler term and an interference term. For the kinematic settings of this experiment, the Bether-Heitler term can be computed with a precision of 1% [7].

In the formalism developed by Belitsky and Müller in [8], the DVCS and interference terms can be expressed as harmonic expansions with respect to the azimuthal angle ϕ defined in Fig. 1 (right). For instance, the DVCS term is of the form:

$$|T_{DVCS}|^2 \propto c_0^{DVCS} + \sum_{n=1}^{2}\left[c_n^{DVCS}\cos(n\phi) + s_n^{DVCS}\sin(n\phi)\right], \tag{1.4}$$

where the coefficients c_n^{DVCS} and s_n^{DVCS} are bi-linear combinations of CFFs depending on the beam helicity.

Using a longitudinally polarized electron beam, at leading twist, the sum and difference of polarized cross sections with opposite beam helicity allow to separate the real and imaginary parts of CFFs contributions to the DVCS amplitude:

$$\frac{d^4\overrightarrow{\sigma} + d^4\overleftarrow{\sigma}}{2} = |BH|^2 + |DVCS|^2 + \mathscr{R}e_{CFF}(I), \tag{1.5}$$

$$\frac{d^4\overrightarrow{\sigma} - d^4\overleftarrow{\sigma}}{2} = \mathscr{I}m_{CFF}(I). \tag{1.6}$$

2. Experiment goal and apparatus

The data acquisition of the experiment took place at Jefferson Lab (Newport News, Virginia, USA), in Hall A, between Fall 2014 and Fall 2016. This experiment has two main goals: perform a scaling test by measuring cross sections with a larger Q^2 lever arm than before, for several values of x_{Bj} (see Fig. 2), and separate the real and imaginary parts of the CFFs contribution to the DVCS amplitude (see Eq. (1.5) and (1.6)) [9].

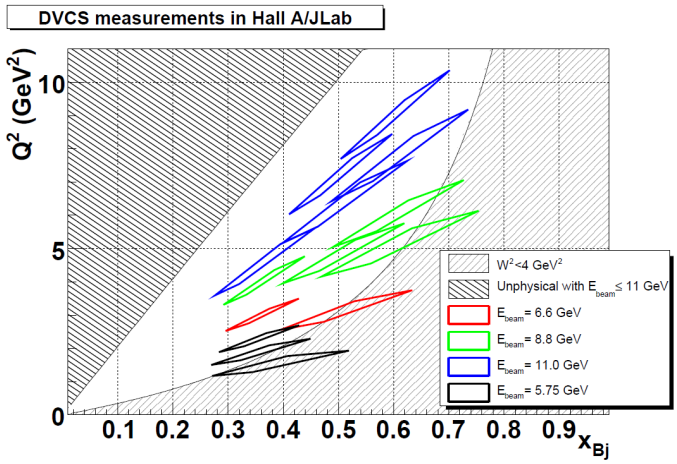

Figure 2: The kinematic regions (Q^2 ; x_{Bj}) explored by this DVCS experiment are represented in red, green and blue. The regions in black were studied during a previous experiment, in 2010.

A longitudinally polarized electron beam was sent on a liquid hydrogen target. The scattered electron was detected in a High Resolution Spectrometer (HRS) while the emitted photon was detected in a custom electromagnetic calorimeter made of 208 PbF_2 crystals. The recoil proton was not detected, however, it was identified by the missing mass $ep \to e'X\gamma$: $M_X^2 = (e+p-e'-\gamma)^2$.

3. Analysis overview

To extract the cross sections, DVCS events must be properly selected. Cuts are applied to the vertex in order to eliminate events occurring in the target aluminum walls. Regarding the photon, only one cluster must be reconstructed in the calorimeter. A cut is applied to its energy in order to eliminate low energy background, and the photon must be far enough from the edges of the calorimeter in order to avoid energy leaks. Regarding the electron, a cut is applied to the energy deposited in the Cherenkov and Pion Rejector detectors of the spectrometer to separate electrons from π^-. A single track must be reconstructed per event, otherwise, associating each track to the correct particle would be very challenging. Finally, a cut is applied to the distance of the electron to the edges of the spectrometer acceptance in order to ensure that the particle is properly reconstructed inside the detector.

Correction factors are applied to take into account experimental inefficiencies and DVCS events discarded by the previous cuts. For instance, corrections are applied for trigger inefficiency, the dead time, the beam polarization, discarded events with multiple tracks in the spectrometer or multiple clusters in the calorimeter, etc...

The cuts described previously are not sufficient in order to select DVCS events and two sources of background need to be taken into account: accidental events and π^0 contamination.

The electron and the photon must be detected in coincidence. As this experiment time resolution is slightly better than 1 ns, it is requested that the photon must be detected within ± 3 ns of the electron. However, these two particles can also come from different events, and be detected in coincidence by accident: they are "accidental events". The probability for accidental photons to be detected within ± 3 ns of the electron is the same as in any other time window of the same width.

Furthermore, the electron beam at Jefferson Lab has a time structure of 4 ns. As a consequence, every photon detected between -11 ns and -5 ns with respect to the electron are accidental, and subtracting these events from the data allows to eliminate the contamination.

In parallel to DVCS, π^0 events $ep \to e'p'\pi^0$ where the π^0 decays into two photons can also be detected. However, if the decay is asymmetric with respect to the π^0 momentum, one of the two photons gets a very low energy and can be missed by the calorimeter. These events are then wrongfully identified as DVCS ones. To subtract this π^0 contamination, one relies on the following method: first, π^0 events are identified in the data by requesting two photons in the calorimeter and an invariant mass compatible with π^0s. Then, for each π^0 identified in the data, its decay into two photons is simulated by a Monte-Carlo technique. The cases where a single photon is detected are contaminating events. As a consequence, the normalized number of simulated events with a single photon detected in the calorimeter are subtracted from the data. Using π^0 detected in the data, this subtraction method takes into account the π^0 production cross section. A cross check with a Geant4 simulation later showed that this method is efficient across the whole surface of the calorimeter except its edges and corners because of acceptance effects. To ensure the efficiency of the subtraction, the photons must be detected far enough from these areas.

Once accidental events and the π^0 contamination have been subtracted, the recoil proton can be identified through the DVCS missing mass $M_X^2 = (e + p - e' - \gamma)^2$. By conservation of energy and momentum, M_X^2 should be equal to the squared mass of the proton (~ 0.88 GeV^2). Selecting events which have a squared missing mass in the 0.88 GeV^2 peak (see Fig. 3) allows to identify the recoil proton and ensures the exclusivity of the DVCS process.

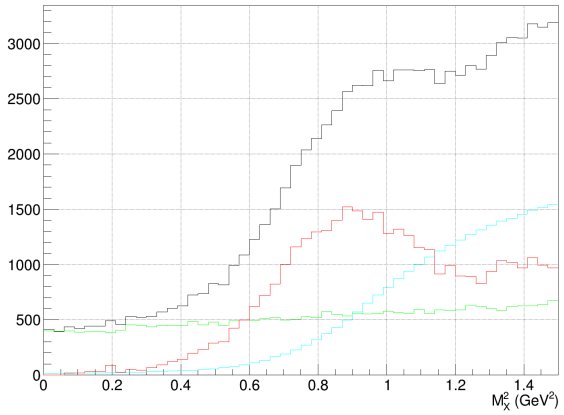

Figure 3: Distribution of the DVCS missing mass $M_X^2 = (e+p-e'-\gamma)^2$. Black: DVCS missing mass before contamination subtraction. Red: DVCS missing mass after accidental and π^0 contamination subtractions. Green: Accidental events. Blue: π^0 contamination.

Semi Inclusive DIS and resonances associated with DVCS can also be wrongfully identified as DVCS events if additional particles are missed ($ep \to e'p'\gamma X$) or if the proton turns into a Δ ($ep \to e'\Delta\gamma$), for instance. In theory, these reactions cannot have a missing mass lower than 1.15 GeV^2 and cutting on M_X^2 should eliminate the contamination. However, because of resolution effects, some contamination can still remain below 1.15 GeV^2 which then becomes a source of systematic uncertainty.

The acceptance is computed with a Geant4 simulation reproducing exactly the geometry of the experimental setup. Furthermore, real radiative corrections are implemented in the simulation to take into account the radiative tail in the acceptance computation. On the other hand, virtual radiative corrections have not been computed yet, but they are expected to be very similar to the previous Hall A experiment [10].

A large number of DVCS events are eliminated by the cuts on the missing mass. This can be compensated by applying the same cuts to the simulation, but its missing mass distribution must reproduce the one from the data. To this end, the simulated photon energy is smeared by a Gaussian Gauss(μ,σ), where the parameters μ and σ depend on the photon position in the calorimeter because of differences between each of its blocks.

4. Cross sections extraction and preliminary results

To extract four-fold cross sections, the DVCS events are sorted into experimental bins in Q^2 (1), x_{Bj} (1), t (5) and ϕ (24) for each kinematic setting. The extraction method relies on a parametrization of the cross section with CFFs combinations, where the CFFs are directly fitted to the experimental number of events. This method presents the advantage of easily taking into account bin migration effects and integrating kinematic dependencies over each bin.

The fitting method consists in minimizing the χ^2:

$$\chi^2 = \sum_{bins} \left(\frac{N_{exp} - N_{simu}}{\sigma_{exp}} \right)^2 \quad \text{with} \quad N_{simu} = L \int \frac{d\sigma}{d\Omega} d\Omega, \tag{4.1}$$

where N_{exp} is the experimental number of events, N_{simu} is the number of events from the Geant4 simulation that must be fitted to the data, L is the integrated luminosity, and σ is the cross section parametrized by CFFs combinations as $\sigma = \sum_n F_n X_n$, where X_n are the CFFs combinations and F_n are kinematic factors. The parametrization relies on the formalism of [8].

The integration of the kinematic factors F_n and bin migration effects are computed with the simulation, and the minimization of Eq. (4.1) with respect to the parameters X_n allows to fit the CFFs combinations to the data. The normalized χ^2 obtained for each kinematic setting were reasonably close to 1. Once the CFFs combinations X_n are fitted, the DVCS cross section can be reconstructed as $\sigma_{fit} = \sum_n F_n X_n^{fit}$.

The main source of systematic uncertainty originates from the cuts on the missing mass, due to remaining contamination from SIDIS and resonances below 1.15 GeV^2, and an imperfect matching of the data and simulation missing mass distributions. The nominal missing mass cuts are chosen so that the agreement between the data and the simulation is as good as possible between them (see Fig. 4). Then, the variations of the cross section with respect to variations of the missing mass cuts around the nominal ones are studied. The maximal variations of the cross section are then taken as point-to-point systematic uncertainties and were found to be between 2% and 5%. They must be quadratically added to the correlated systematic uncertainties which were evaluated around 3% (preliminary).

Examples of the preliminary cross section measurements are displayed in Fig. 5. The unpolarized cross section can be distinguished from the Bethe-Heitler and a sizable DVCS contribution can be measured. In particular, for ϕ close to 180° the twist-2 DVCS term is dominant, while for

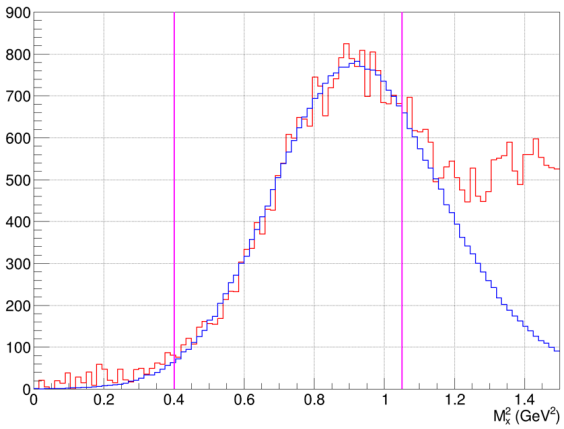

Figure 4: The experimental (simulation) missing mass distribution is represented in red (blue). The magenta lines represent the nominal cuts on the missing mass.

values of ϕ close to 0° and 360°, the twist-2 interference term becomes of comparable size. For both unpolarized and helicity-dependent cross sections, the twist-2 CFF contributions are dominant while the twist-3 ones are close to 0.

The measured cross sections have been compared to two global fits of DVCS data: KM10a and KM15. The model KM10a did not use Hall A data, while the model KM15 includes Hall A and CLAS data up to 2015 [11, 12]. An executable developed by K. Kumerički and D. Müller in order to compute cross sections for each model is available at http://calculon.phy.hr/gpd/. For every kinematic setting, regarding unpolarized cross sections, the data are in a very good agreement with the model KM15, while they are undershot by the model KM10a. Regarding the helicity-dependent cross sections, the data tend to be fairly well described by both fits KM10a and KM15.

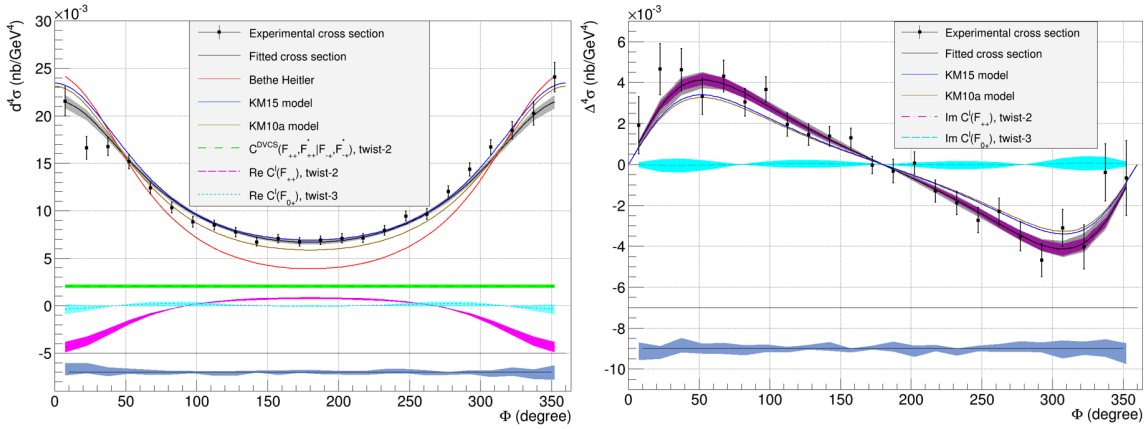

Figure 5: Left (right): unpolarized (polarized) cross section, with $E_{beam} = 8.5$ GeV, $\langle Q^2 \rangle = 3.6$ GeV^2, $\langle x_{Bj} \rangle = 0.36$ and -0.351 GeV$^2 < t < -0.289$ GeV^2. The black dots represent the experimental cross section while the black curve is the cross section fit, with statistical uncertainties. The Bethe-Heitler is represented in red, while the models KM10a and KM15 are respectively in brown and blue. The contributions of the CFFs combinations F_nX_n are represented in green, magenta and cyan, with their respective statistical uncertainties. The blue band at the bottom represents the systematic uncertainty from the missing mass cuts.

5. Conclusion and outlook

This experiment was the first one to be performed at Jefferson Lab since the upgrade of the accelerator facility at 12 GeV. Preliminary unpolarized and polarized DVCS cross sections have been measured over 9 kinematic settings and 120 experimental bins each, for a total of 1080 new data points. The contributions of CFFs combinations to the cross sections have also been extracted.

The optimization of the simulation smearing, the study of the Q^2 and t-dependence of the CFFs, and the finalization of systematic uncertainties are work in progress. Finalized results are expected in the near future.

References

[1] X.-D. Ji, *Gauge-Invariant Decomposition of Nucleon Spin and Its Spin-Off*, Phys. Rev. Lett. 78, 610 (1997) [hep-ph/9603249].

[2] A.V. Radyushkin, *Nonforward parton distributions*, Phys. Rev. D 56, 5524 (1997) [hep-ph/9704207].

[3] D. Mueller, D. Robaschik, B. Geyer, F.M. Dittes and J. Horejsi, *Wave Functions, Evolution Equations and Evolution Kernels from Light-Ray Operators of QCD* Fortsch. Phys. 42, 101 (1994) [hep-ph/9812448].

[4] X.-D. Ji and J. Osborne, *One loop corrections and all order factorization in deeply virtual Compton scattering*, Phys. Rev. D 58, 094018 (1998) [hep-ph/9801260].

[5] J. C. Collins and A. Freund, *Proof of factorization for deeply virtual Compton scattering in QCD*, Phys. Rev. D 59, 074009 (1999) [hep-ph/9801262].

[6] A. Bacchetta, U. D'Alesio, M. Diehl and C. A. Miller, *Single-spin asymmetries: the Trento conventions*, Phys. Rev. D70,117504 (2004) [arXiv:hep-ph/0410050].

[7] J. J. Kelly, *Simple parametrization of nucleon form factors*, Phys. Rev. C 70, 068202 (2004).

[8] A. V. Belitsky, D. Müller, and Y. Ji, *Compton scattering: from deeply virtual to quasi-real*, Nucl. Phys. B878, 214-268 (2014) [arXiv:1212.6674].

[9] J. Roche, C. E. Hyde-Wright, B. Michel, C. Munoz Camacho, et al. (The Jefferson Lab Hall A Collaboration) *Measurements of the Electron-Helicity Dependent Cross Sections of Deeply Virtual Compton Scattering with CEBAF at 12 GeV*, PR12-06-114 (2006) [nucl-ex/0609015].

[10] M. Defurne et al. (Jefferson Lab Hall A Collaboration) *The E00-110 experiment in Jefferson Lab's Hall A: Deeply Virtual Compton Scattering off the Proton at 6 GeV*, Phys. Rev. C 92, 055202 (2015) [arXiv:1504.05453].

[11] K. Kumerički and D. Müller *Description and interpretation of DVCS measurements*, EPJ Web of Conferences 112, 01012 (2015) [arXiv:1512.09014].

[12] K. Kumerički, S. Liuti and H. Moutarde *GPD phenomenology and DVCS fitting*, Eur. Phys. J. A. 52, 157 (2016) [arXiv:1602.02763].